Science of the Total Environment 663 (2019) 45–59

Contents lists available at ScienceDirect

Science of the Total Environment

journal homepage: www.elsevier.com/locate/scitotenv

Impact of physiological and phenological change on carbon uptake on the Tibetan Plateau revealed through GPP estimation based on spaceborne solar-induced fluorescence

Shiliu Chen [a,*], Yuefei Huang [a,b,**], Shuai Gao [a], Guangqian Wang [a]

[a] State Key Laboratory of Hydroscience and Engineering, Department of Hydraulic Engineering, Tsinghua University, Beijing 100084, China
[b] State Key Laboratory of Plateau Ecology and Agriculture, Qinghai University, Xining, Qinghai 810016, China

HIGHLIGHTS

- Gross primary production (GPP) is estimated with SIF space observations on the TP.
- An assemble of SGS, GPP_{max} and EGS can explain 72 ± 20% of GPP inter-annual variability.
- GPP variability is dominated by physiology in the most areas of the TP.
- The response of GPP to phenological and physiological change has altitude dependence.
- The response of phenology and physiology to climate variations has spatial heterogeneity.

GRAPHICAL ABSTRACT

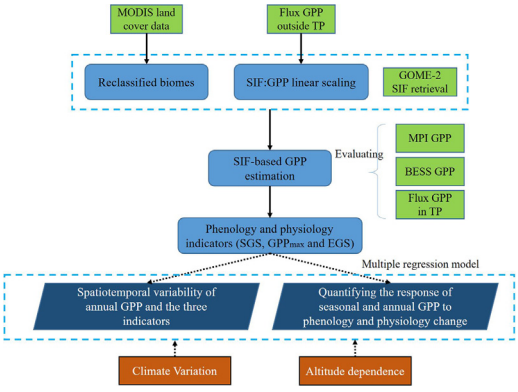
MODIS land cover data
Flux GPP outside TP
Reclassified biomes
SIF:GPP linear scaling
GOME-2 SIF retrieval
SIF-based GPP estimation
Evaluating
MPI GPP
BESS GPP
Flux GPP in TP
Phenology and physiology indicators (SGS, GPPmax and EGS)
Multiple regression model
Spatiotemporal variability of annual GPP and the three indicators
Quantifying the response of seasonal and annual GPP to phenology and physiology change
Climate Variation
Altitude dependence

ARTICLE INFO

Article history:
Received 22 November 2018
Received in revised form 18 January 2019
Accepted 20 January 2019
Available online 26 January 2019

Editor: Elena Paoletti

Keywords:
Gross primary production (GPP)
Fluorescence
Phenology
Photosynthetic capacity
Climate change
Tibetan plateau

ABSTRACT

Although gross primary production (GPP) is an essential proxy for reflecting terrestrial ecosystem function, GPP estimation at regional scale on the Tibetan Plateau (TP) is constrained by the lack of ground observations. Moreover, how climate-induced phenological and physiological change further affects carbon uptake in this region remains unclear. In this study, we first estimated GPP at 8-day intervals and a 0.5° resolution from 2007 to 2015 over the TP based on an improved approach and GOME-2 sun-induced fluorescence (SIF) retrievals. The obtained SIF-based GPP coincided well with flux observations and two state of the art GPP products, with a regional carbon uptake of 0.62 ± 0.04 PgC $year^{-1}$ or 307 ± 22 gC m^{-2} $year^{-1}$. With the SIF-based GPP, two phenological indicators (start and end date of the growing season, i.e., SGS and EGS) and one physiological indicator (maximum photosynthesis capacity, GPP_{max}) were identified and their relative contributions to inter-annual GPP variability were further quantitatively separated using a multiple regression model. Advanced SGS, delayed EGS, and increasing GPP_{max} can all enhance carbon uptake and a combination of the three indicators can explain 72 ± 20% of GPP inter-annual variability. The response of annual GPP to phenological and physiological variations has significant altitude dependence, as the decline of annual GPP in most of the area is dominated by the GPP_{max} decline, while the increase of annual GPP in the high-altitude area is dominated by the advanced SGS. The response of all three indicators to both temperature and precipitation variation has great spatial heterogeneity.

* Corresponding author.
** Correspondence to: Y. Huang, State Key Laboratory of Hydroscience and Engineering, Department of Hydraulic Engineering, Tsinghua University, Beijing 100084, China.
E-mail addresses: csl16@mails.tsinghua.edu.cn (S. Chen), yuefeihuang@tsinghua.edu.cn (Y. Huang).

https://doi.org/10.1016/j.scitotenv.2019.01.324
0048-9697/© 2019 Elsevier B.V. All rights reserved.

Our study suggests that remote sensing of SIF can provide a unique opportunity to estimate GPP in regions with a lack of ground observations and that our enhanced understanding of the impact of the climate-induced phenological and physiological change on GPP variability in alpine ecosystems can improve GPP estimation in a changing climate.

© 2019 Elsevier B.V. All rights reserved.

1. Introduction

Plants in terrestrial ecosystems absorb carbon dioxide (CO_2) and produce organic compounds through photosynthesis, regulating the carbon cycle and balance globally (Beer et al., 2010; Pan et al., 2011; Piao et al., 2009). Carbon assimilation in this process is quantified as gross primary production (GPP) at the ecosystem level (Beer et al., 2010). As the world's largest carbon flux, terrestrial ecosystem GPP, coupled with water and energy, is the major driver of ecosystem function (Ballantyne et al., 2012; Beer et al., 2010; Jung et al., 2011). This process provides the basis of food and energy for all life on earth (Guanter et al., 2014) and offsets CO_2 emissions (Piao et al., 2009).

Known as the "World's Roof," the Tibetan Plateau (TP) is a unique region attracting a significant amount of research interests related to the following aspects of ecology and hydrology. Firstly, the TP has the largest and highest alpine ecosystem in the world, covering a quarter of China (about 2.5 million km^2) and dominated by alpine grass (meadow and steppe) that accounts for 44% of the grassland in China (Chen et al., 2013). Secondly, the TP has a vital and irreplaceable ecological function (Chen et al., 2013; Piao et al., 2011; Zhang et al., 2018). As the headwaters of three major rivers in China (i.e. the Yangtze River, the Yellow River and the Lancang River) generates from the TP, its ecological conservation is particularly important. Thirdly, due to its unique vegetation composition and climate features, TP's ecosystem is inherently fragile and unstable (Chen et al., 2013; Piao et al., 2011; Shen et al., 2015; Zhang et al., 2018). Moreover, featured by a cold and dry climate in most areas, the TP is one of the most sensitive regions to climate change (Che et al., 2014; Wang et al., 2017; Zhang et al., 2018). On the TP, climate change has induced changes in the terrestrial carbon cycle (Chen et al., 2013; Gao et al., 2013), hydrological cycle (Zhang et al., 2016a), and in vegetation phenology and physiology (Yu et al., 2010). Finally, given the large area of the TP, carbon uptake in this region plays an important role for global carbon balance and CO_2 emission offsetting, as both site observations (Kato et al., 2004; Kato et al., 2006; Zhao et al., 2006) and model simulation results (Zhuang et al., 2010) suggest that the TP has functioned as a carbon sink in recent years. Hence, obtaining robust GPP estimation and a deeper understanding of the mechanism for GPP variability on the TP is imperative (Gao et al., 2014; Kato et al., 2006; Li et al., 2007; Zhao et al., 2006).

The carbon uptake (GPP) of vegetation is jointly controlled by both phenological and physiological processes (Richardson et al., 2009; Xia et al., 2015; Zhou et al., 2016; Zhou et al., 2017). Since phenology is sensitive to temperature (Keenan et al., 2014) and the TP has experienced significant temperature increases over the past decades (Wang et al., 2017), warming-induced phenological change on the TP has attracted significant attentions (Cong et al., 2016; Shen et al., 2016). However, independent studies have suggested different phenological responses to climate change in this region (Cong et al., 2016; Shen, 2011; Wang et al., 2017; Yu et al., 2010). Though physiological change attributed to climate change can be expected on the TP, relevant research is rare (Fu et al., 2015). While the coupling of carbon uptake to phenology and physiology has been revealed across the Americas and Europe (Keenan et al., 2014; Richardson et al., 2009; Xia et al., 2015; Zhou et al., 2016; Zhou et al., 2017), there is still little understanding of how phenological and physiological change affects carbon uptake on the TP. Given the projected future climate change on the TP (Piao et al., 2011) and its ecological importance (Chen et al., 2013), it is essential to understand how climate change affects GPP variability through phenological and physiological processes in this region.

Though the limited flux towers on the TP provide GPP observations, they are constrained at site or landscape levels (Kato et al., 2004; Li et al., 2016; Zhao et al., 2006), and spatially explicit GPP estimation in this region is still restricted by two major factors: a lack of ground observations and large spatial heterogeneity (Gao et al., 2014; Li et al., 2007; Zhang et al., 2008). Conventional approaches to estimate spatial explicit GPP are based on either data-oriented or process-based models (Beer et al., 2010; Gao et al., 2014; Jung et al., 2011; Li et al., 2007). However, the inadequate calibration and validation of model parameters and empirical algorithms, which can be attributed to the limited ground observations obtained on the TP, is associated with significant GPP simulation uncertainties for both model types (Gao et al., 2014, Li et al., 2007, Zhang et al., 2008). Moreover, the huge spatial heterogeneity on the TP, primarily attributed to the dramatic spatial variance in geographical features (e.g. altitude, Fig.S1), climate background (e.g., temperature and precipitation, Fig.S1) and water condition (e.g., soil moisture) (Zeng et al., 2015), constrains the application of the algorithms or parameters inferred at site level to the whole region (Piao et al., 2011).

Recent advances in remote sensing offer the unique opportunity to map spatially explicit GPP for regions that lack ground observations. During the plant photosynthetic process, chlorophyll fluorescence is induced by solar radiation (Joiner et al., 2014). Hence, solar-induced fluorescence (SIF) can accurately track the seasonal cycle of GPP (Joiner et al., 2014). Space observation SIF retrieval can be obtained with the development of spectroscopy (Joiner et al., 2013; Köhler et al., 2015) and its great potential for GPP estimation has been well validated (Guan et al., 2016; Guan et al., 2017; Guanter et al., 2014; Joiner et al., 2014; Sun et al., 2017). SIF-based GPP estimation is reported to have much better performance than other GPP products in the US Corn Belt (Guan et al., 2016; Guan et al., 2017; Guanter et al., 2014). However, the existing approaches to derive SIF-based GPP cannot be applied directly to the TP due to the lack of ground observations.

Therefore, we aim to improve the existing method to coordinate with the data limitation in the TP so that the potential of GPP estimation for the TP based on SIF retrievals will be explored. The impact of phenology and physiology on GPP variability during 2007–2015 was also quantitatively separated in this study based on our SIF-derived GPP and a multiple regression model. Specifically, our objectives (Fig. 1) were (1) to estimate GPP on the TP based on our improved approach with GOME-2 SIF retrievals and reclassified land cover data; (2) to compare our SIF-based GPP with flux observations and other estimation approaches; (3) to derive the phenological and physiological indicators and investigate their spatiotemporal variability; (4) to quantitatively separate the impact of phenology and physiology on GPP variability; and (5) to estimate the impact of climate variation and altitude dependence on the response of GPP to phenological and physiological change.

2. Method and materials

2.1. Land cover reclassification

Here we used the MODIS land cover data (MCD12C1) from 2007 to 2015 based on the IGBP classification at 500 m and an annual scale (Friedl et al., 2002). It was produced by interpreting the MODIS imagery based on global training sites and ancillary data with a supervised

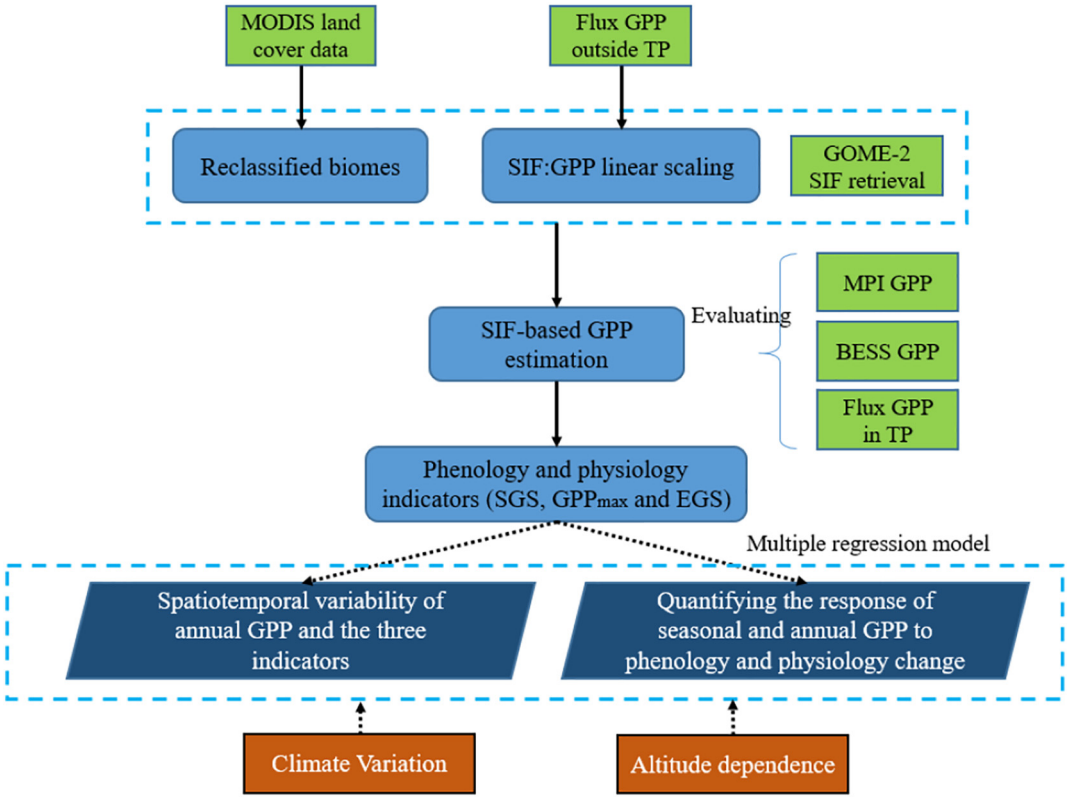
MODIS land cover data
Flux GPP outside TP
Reclassified biomes
SIF:GPP linear scaling
GOME-2 SIF retrieval
SIF-based GPP estimation
Evaluating
MPI GPP
BESS GPP
Flux GPP in TP
Phenology and physiology indicators (SGS, GPPmax and EGS)
Multiple regression model
Spatiotemporal variability of annual GPP and the three indicators
Quantifying the response of seasonal and annual GPP to phenology and physiology change
Climate Variation
Altitude dependence

Fig. 1. Flowchart illustrating the approaches used to estimate SIF-based GPP and quantify the impact of physiological and phenological change on GPP.

classification method (Friedl et al., 2002). As plateau grassland (steppe and meadow) and barren land occupy the majority of the TP (Piao et al., 2011) and other vegetation only covers a small proportion of area, the original IGBP-based land cover classification was reclassified into six biomes based on biomass (Table S1): forest (FOR), shrublands and savannas (SAS), grassland (GRA), cropland (CRO), non-vegetated land (NVL), and barren or sparsely vegetated land (BSV). Then, the MODIS land cover data was integrated into 0.5° to match the SIF spatial resolution. The area proportion of six biomes in each pixel was calculated and averaged into a multi-year value. The dominant biome in the TP is GRA, followed by BSV, NVL, FOR, SAS, and CRO, covering 56.3%, 33.7%, 3.9%, 3.1%, 2.5%, and 0.5% of the area, respectively (Fig. 2), which agrees well with Piao et al. (2011). As BSV and NVL nearly have no vegetation and the CRO area proportion is too small, we only focused on the other three biomes, i.e., GRA, FOR, and SAS.

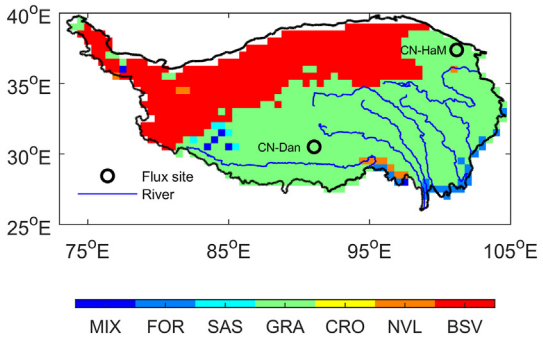

Fig. 2. Spatial distribution of the biomes based on the reclassification of MODIS land cover data on the TP. The black circles indicate the two used flux tower sites (CN-Dan and CN-HaM). FOR, SAS, GRA, CRO, NVL, and BSV refer to different reclassified biomes, i.e., forest, shrublands and savannas, grassland, cropland, non-vegetated land, and barren or sparsely vegetated land, respectively. The pixels, whose fraction of each biome do not exceed 40%, are defined as mixed biomes (MIX).

2.2. GPP estimation with SIF retrievals

A new version of GOME-2 SIF retrievals developed by Köhler et al. (2015) was used to estimate GPP on the TP. Launched in 2006, GOME-2 can measure wavelengths between 240 and 790 mm using four detector channels, and samples near 9:30 a.m. locally with a footprint of 40 × 80 km^2 (Joiner et al., 2013; Joiner et al., 2014; Köhler et al., 2015). Based on the inversion of the measurements at a sub-channel (720 and 758 nm) of GOME-2, SIF retrieval is evaluated at 740 nm (Köhler et al., 2015). The GOME-2 SIF dataset can be obtained at daily scale and a 0.5° resolution from 2007 to 2015 (Köhler et al., 2015). Following Joiner et al. (2014), since the daily global map of SIF is incomplete, we averaged the daily SIF into 8-day intervals to obtain a complete map for the TP.

Given the inherent mechanism linkage between SIF and GPP, many studies have attempted to estimate GPP with SIF retrieval (Guan et al., 2016; Guanter et al., 2014; Lee et al., 2013; Sun et al., 2017) using two common approaches. Guanter et al. (2014) built the empirical linear relationship between raw SIF and flux tower GPP to directly scale SIF retrievals into GPP. However, this method does not consider the different linear SIF-GPP scaling for C3 and C4 plants because of their different photosynthetic pathways (Guan et al., 2016; Zhang et al., 2014). Hence, Guan et al. (2016) developed a more mechanistic method upon the work by Guanter et al. (2014), using different electron use efficiencies (EUEs) for C3 and C4 crops, respectively. Since the majority of vegetation on the TP is C3 plants (i.e., C3 grass and C3 forest) (Collatz et al., 1998; Still et al., 2003), the previous two approaches make no difference in terms of estimation performance. Thus, we chose the method by Guanter et al. (2014) as it required fewer input data, making it feasible for use in the TP region.

The light use efficiency (LUE) model developed by Monteith (1972) is a widely used approach for GPP modeling (Running et al., 2000):

$$GPP = aPAR \times LUE_{GPP} \quad (1)$$

where *aPAR* and LUE_{GPP} refer to the absorbed photosynthetic active radiation by the canopy and the transforming efficiency from aPAR to GPP, respectively. As for SIF, it can be conceptualized with a similar LUE model (Guanter et al., 2014; Sun et al., 2017):

$$SIF = aPAR \times LUE_{SIF} \times \alpha \quad (2)$$

where the term LUE_{SIF} is similar to LUE_{GPP}, referring to the fraction of aPAR converting to SIF and term α indicates the fraction of SIF escaping from canopy to be measured by satellite. By combining Eq. (1) with Eq. (2), we can obtain the relationship between SIF and GPP:

$$GPP = SIF \times \frac{LUE_{GPP}}{LUE_{SIF} \times \alpha} \quad (3)$$

Based on the mechanism described by Eq. (3), many previous works have empirically obtained the SIF-GPP linear relationship by comparing SIF retrievals and flux GPP and the results have been well validated (Guanter et al., 2014; Sun et al., 2017; Zhang et al., 2016b). Though this empirical approach is not mechanistic as a biophysical model, it provides a feasible framework to link GPP with SIF. The empirical SIF-GPP linear relationship is reported to be universal cross sites of the same biome (Guanter et al., 2014) even cross biomes (Sun et al., 2017). Given LUE_{GPP}, LUE_{SIF} and α would vary with the environment, photosynthetic capacity, and canopy structure (Running et al., 2000; Sun et al., 2017), we hypothesized that the SIF-GPP relationship varies across biomes. Thus, we first estimated the empirical relationship between SIF retrieval and flux GPP for the three major biomes, respectively. Unfortunately, the data records of all three sites on the TP (i.e., CN-Dan, CN-HaM, and CN-Ha2, Table.S2) do not overlap with the period of SIF data (2007–2015). Hence, we assumed that sites from the same biome and similar climatic environments have similar SIF-GPP relationships (Guanter et al., 2014) and chose GPP observations from sites outside the TP with the same biome type and similar environmental conditions. As flux observation exhibits a different footprint with satellite SIF retrieval (1–2 km for flux data vs 0.5° for SIF), we only selected the flux sites whose corresponding SIF pixels have the same and relatively uniform land cover (area proportion of the dominant biome larger than 60% and a coefficient of variation of enhanced vegetation index (EVI) <0.2). According to the criteria above, 11 flux sites were chosen (Table.S2, three for GRA, five for FOR, and three for SAS) from FLUXNET2015 Dataset. The FLUXNET2015 Dataset (http://fluxnet.fluxdata.org/data/fluxnet2015-dataset/) contains data from global flux tower sites; the data quality control and processing have been improved upon from previous versions.

To further reduce the uncertainty due to scale mismatch, both SIF and flux GPP were averaged as multi-year mean values at 8-day intervals to estimate the empirical SIF-GPP relationship, with negative flux GPP and its corresponding SIF removed (Guanter et al., 2014; Joiner et al., 2014). The SIF-GPP relationship was first estimated at each site. SIF performed strongly in capturing the seasonality of GPP, with a strong linear correlation with flux GPP (except US-SRC, R^2 of all sites >0.8, Fig. S2). Though SIF-GPP linear scaling differs slightly at different sites, it has a similar SIF-GPP relationship at sites with the same biome. Thus, we lumped data from all sites of the same biome to build a simple universal SIF-GPP relationship for each biome. As depicted in Fig. 3, the SIF-GPP linear scaling of different biomes exhibited a significant discrepancy, which proved our hypothesis. The significantly strong SIF-GPP linear relationship for each biome suggests that a universal SIF-GPP linear scaling with different sites assembled is feasible for linking SIF with GPP for the same biome. However, we should note that there is a slight decrease of R^2 and more scatter plots (Fig. 3) compared with the SIF-GPP relationship at a single site (Fig. S2), which can be attributed to the slight difference in the SIF-GPP relationship at various sites. Hence, we used the estimated 95% confidence interval (the red dashed line in Fig. 3) to quantify the uncertainties introduced by using the universal SIF-GPP relationship for the same biome (shown in Fig. S5) and further evaluated our estimation with state-of-art GPP products.

We then improved the method by Guanter et al. (2014) by applying different scaling for different biomes to map spatially explicit GPP on the TP based on the area fraction of each biome in one pixel, as shown in Eq. (4).

$$GPP = SIF \times LS_i \times Fra_i \quad (4)$$

where *i* denotes different biomes and *LS* and *Fra* denote the SIF-GPP linear scaling and area fraction of each biome in one pixel. Here we assumed that the land use did not change in our study period and the pixels with (NVL + BSV) > 40% were neglected.

2.3. Evaluating the SIF-based GPP

Our SIF-based GPP was first evaluated with flux observations from the TP and then compared with other GPP estimations on the TP. With regard to a new spatially explicit GPP estimation approach on the TP, the key issue is how effectively it can capture the spatiotemporal variability and absolute value of GPP in this region. Therefore, we used two statistical metrics, determination coefficient (R^2) and normalized root mean square error (NRMSE), to evaluate its performance.

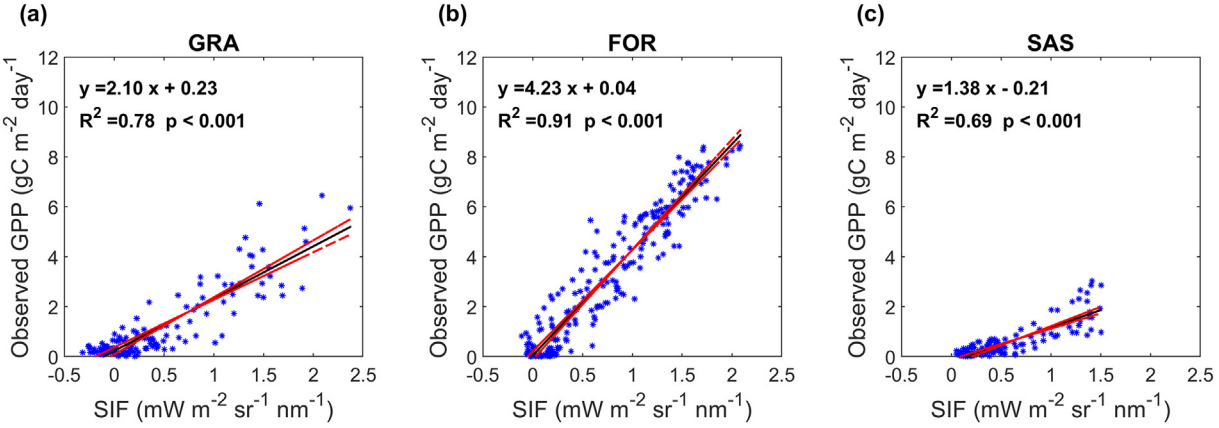

Fig. 3. Linear scaling between SIF retrieval and flux GPP observation for the three major biomes on the Tibetan Plateau, with (a) for grassland (GRA), (b) for forest (FOR) and (c) for shrub land and savannas (SAS), respectively. Each symbol indicates the multi-year averaged values at 8-day intervals during the overlap of SIF data and available flux observations, for a SIF pixel and its corresponding flux tower site. The negative flux GPP have been removed so that the corresponding SIF were not used.

We compared our SIF-based GPP with two state-of-the-art GPP products, MPI GPP (Max Planck Institute for Biogeoschemistry) from a data-oriented model and BESS GPP (Breathing Earth System Simulator) from a process-based model. MPI GPP is mapped by upscaling FLUXNET observations to a global scale through machine learning methods using satellite vegetation indices, meteorological data, and land use data as inputs (Jung et al., 2011). BESS is based on a simplified biophysical model that considers atmosphere and canopy radiative transfers and canopy photosynthesis-transpiration-energy balance. BESS requires MODIS atmospheric and land products as inputs (Jiang and Ryu, 2016; Ryu et al., 2011). Though the three GPP products all rely on remote sensing data, they have independent satellite data as inputs and their algorithms are different (details in Table.S3). Our SIF-based GPP is based on an independent satellite dataset, GOME-2 SIF, which avoids the same systematical biases displayed by the other two products. Moreover, both MPI GPP and BESS GPP agree well with site-observations and exhibit better performance than other GPP products. Thus, they are appropriate for cross-validation of the SIF-based GPP product (Guan et al., 2016; Guanter et al., 2014; Jiang and Ryu, 2016; Jung et al., 2011; Ryu et al., 2011). MPI GPP and BESS GPP both have a 0.5° resolution on a monthly scale and their overlap periods with SIF-based GPP were from 2007 to 2011 and 2007 to 2015, respectively.

2.4. Deriving phenological and physiological metrics

To investigate the impact of phenology and physiology on carbon uptake, we needed to derive the phenological and physiological metrics. Generally, this consists of two steps (Cong et al., 2012; Piao et al., 2006): (1) fitting a smooth phenology curve with satellite signals and (2) determining the phenological and physiological metrics with a threshold based on the fitted curve.

2.4.1. Fitting phenology curve

Different algorithms have been developed to reconstruct a smooth phenology curve at a daily interval based on the satellite products time series (Cong et al., 2012; White et al., 2009). Generally, vegetation in different regions has different phenological features and requires different approaches (Cong et al., 2012; Xia et al., 2015). As the seasonal cycle of vegetation in the TP is a one-peak curve during the growing season (Zhang et al., 2018), obtaining a robust result required the use of two algorithms suitable for one-peak curve to reconstruct the GPP time series: the Gaussian method by White et al. (2009) and Polyfit method by Piao et al. (2006). The Gaussian method uses a simple Gaussian curve as follows:

$$GPP(t) = a + b \times e^{-\left(\frac{t-c}{d}\right)^2} \quad (5)$$

where $GPP(t)$ is the fitted daily GPP at time t and a, b, c, and d are the fitted coefficients. The Polyfit method is based on a six-degree polynomial function as follows:

$$GPP(t) = a_0 + a_1 t^1 + a_2 t^2 + a_3 t^3 + a_3 t^3 + a_3 t^3 + a_6 t^6 \quad (6)$$

where $a_1, \ldots, a_6$ are the fitted coefficients. To eliminate the impact from clouds or other data uncertainties, we applied the Savitzky-Golay (SG) smoothing model to filter outliers before fitting the phenology curve.

2.4.2. Determining the phenological and physiological metrics

The start and end date of the growing season (i.e., SGS and EGS) are two widely used metrics for phenological research, considered as indicators of the spring emergence and autumn senescence, respectively (Cong et al., 2012; Keenan et al., 2014; Richardson et al., 2010). As for the physiological metric, Xia et al. (2015) used the maximal daily gross photosynthesis during the growing season (GPP_{max}) to represent the plant physiological properties. Once the seasonal curve is fitted on a daily scale, the peak value can be regarded as GPP_{max} and the phenological metrics can be estimated based on two types of threshold (Piao et al., 2011): (1) a fixed threshold as a percentage of the amplitude or maximum and (2) a dynamic threshold as the maximum increasing/decreasing rate. As different thresholds only affect the specific dates of the phenological metrics but not their inter-annual variability (Keenan et al., 2014; Zhou et al., 2016), we defined the threshold as 10% of the multi-year averaged GPP_{max} for each pixel and determined SGS and EGS as the first day that the daily GPP exceeds and drops down the threshold respectively following the method by Keenan et al. (2014).

Consistent with previous works (Cong et al., 2012, White et al., 2009), the results derived through different reconstruct approaches exhibit similar spatial-temporal characteristics (Fig. S3), despite the date difference between the phenological indicators. Hence, we chose only the result generated using the Gaussian method for further analysis.

2.5. Statistical model to explain GPP variability with hybrid impact of phenology and physiology change

Xia et al. (2015) built a simple model with the length of the carbon uptake period (CUP) within a year and GPP_{max} as the indicator of phenology and physiology respectively (i.e., GPP = CUP × GPP_{max}) and found it can explain >90% of the spatiotemporal GPP variability. As it cannot separate the impact of spring and autumn phenology on GPP variability with the CUP indicator only, Zhou et al. (2016) developed a statistical model based on the work of Xia et al. (2015) as follows:

$$GPP = f(SGS, GPP_{max}, EGS) \quad (7)$$

As the three indicators are assumed to be independent of each other, Eq. (7) can be derived into a total differential format:

$$dGPP = \frac{\partial GPP}{\partial SGS} dSGS + \frac{\partial GPP}{\partial GPP_{max}} dGPP_{max} + \frac{\partial GPP}{\partial EGS} dEGS \quad (8)$$

As the partial derivatives represent the sensitivity of annual GPP to the variation of the three indicators, we can assume that the partial derivatives are constant since they will remain stable during a certain time period (Keenan et al., 2014) and replace them with the sensitivity coefficients α_{SGS}, α_{max}, α_{EGS}, respectively. Besides, the differentials of the four variables are approximated by difference expressions (Δ) on a multi-year average level. Hence, we can convert Eq. (8) into Eq. (9) as follows:

$$\Delta GPP = \alpha_{SGS} \Delta SGS + \alpha_{max} \Delta GPP_{max} + \alpha_{EGS} \Delta ESG \quad (9)$$

Based on this multiple regression model, the sensitivity coefficients can be estimated with our SIF-based GPP and derived indicators to quantify the response of annual GPP to phenological and physiological variations. As GPP has positive response to both advanced SGS and delayed EGS, we used 365-SGS instead of SGS to make coefficients generated for SGS and EGS comparable.

Furthermore, we separated the relative contribution of each indicator to GPP inter-annual variability based on ANOVA analysis. The ANOVA analysis can only calculate the absolute value of relative contribution, but the contribution can be positive or negative. Thus, the contribution is regarded as positive when the trend slope and sensitivity coefficient of the indicator have the same sign, suggesting that its variations lead to increasing GPP and vice versa.

2.6. Climate dataset

The precipitation and temperature data were obtained from the China Meteorological Data Service System (http://data.cma.cn/). They were generated by interpolating the daily ground observations from 2472 stations across China into 0.5° spatial resolution with thin plate spline method based on digital elevation (Hutchinson, 1998a; Hutchinson, 1998b).

3. Results

3.1. Comparison with flux observations

Though the records of the three sites on the TP have no overlap with the SIF-based GPP, we compared their multi-year averaged seasonal curves to evaluate our SIF-based GPP (Joiner et al., 2014). We focused only on the two grass sites on the TP (i.e., CN-HaM and CN-Dan) that fulfill the homogeneity criterion. For the CN-HaM site, the SIF-based GPP agrees well with the observed flux GPP in terms of seasonal dynamics ($R^2 = 0.97$, $p < 0.001$, Fig. 4a) and magnitude (NRSME = 0.35, Fig. 4b). As for the CN-Dan site, we noted that the SIF-based GPP drops earlier compared to the flux GPP (Fig. 4d). This discrepancy may be attributable to the different footprints and periods between the SIF retrieval and flux data (Li et al., 2007). To devise a method for assessing the potential reasons, we further added MPI GPP and BESS GPP into the comparison, which has the same spatial resolution and overlap as the SIF-based GPP. As shown in Fig. S4, both MPI and BESS GPP capture the seasonality of the observed GPP better than the SIF-based GPP at CN-Dan site, indicating that SIF-based GPP has slightly worse performance in capturing seasonality at this site. However, despite this slight discrepancy, the SIF-based GPP shows good overall performance in capturing the seasonal cycle and magnitude at the CN-Dan site ($R^2 = 0.86$, NRSME = 0.72, $p < 0.001$, Fig. 4c, d).

3.2. Comparison with GPP estimation from the process-based model and data-oriented model

The SIF-based GPP estimation was further compared with MPI GPP from the data-oriented model and BESS GPP from the process-based model. Firstly, their time series at each pixel were compared for temporal dynamics (Fig. 5a, b); the SIF-based GPP agreed well with both MPI GPP and BESS GPP, with $R^2 = 0.77 \pm 0.23$ and $R^2 = 0.76 \pm 0.19$, respectively. Only a few pixels with barren land cover located in the west part of the TP presented low correlation coefficients. However, since there is a lack of observations available to develop a benchmark, it is difficult to identify which GPP product captures the 'true' carbon flux. Secondly, the multi-year averaged GPP at each pixel was compared for spatial variability (Fig. 5c, d). Again, the SIF-based GPP exhibit great consistency with both MPI GPP ($R^2 = 0.88$, NRSME = 0.31) and BESS GPP ($R^2 = 0.90$, NRSME = 0.32). Thirdly, all of the monthly values from all pixels were lumped for comparison (Fig. 5e, f), and consistency of the SIF-based GPP with both MPI GPP ($R^2 = 0.78$, NRSME = 0.41) and BESS GPP ($R^2 = 0.82$, NRSME = 0.48) suggests that it can capture not only the spatiotemporal variability but also the absolute value of GPP on the TP.

3.3. Spatiotemporal variabilities of annual GPP and phenological and physiological indicators

The spatiotemporal variability of annual GPP and phenological and physiological indicators (i.e., SGS, GPP_{max}, and EGS) on the TP is illustrated in Fig. 6. All four variables present a similar spatial distribution and exhibit a significant gradient from east to west in the region. Specifically, the maximum annual GPP (750 gC m^{-2} $year^{-1}$) and GPP_{max} (10 gC m^{-2} day^{-1}) and the earliest SGS and latest EGS (date of year (DOY), i.e., DOY = 100 and 300, respectively) appear in the east, while the minimum annual GPP and GPP_{max} and the latest SGS and earliest EGS appear in the west. The regional average annual GPP and GPP_{max} were 307 ± 22 gC m^{-2} $year^{-1}$ and 4.14 ± 0.07 gC m^{-2} day^{-1}, respectively, with a total carbon uptake of 0.62 ± 0.04 PgC $year^{-1}$ (the 95% confidence intervals of annual GPP, as shown in Fig. S5). Meanwhile, the regional averaged DOY of SGS and ESG was 148 and 264, respectively. The range of SGS (114–169, at 90% confidence interval hereafter) and EGS (250–294) agree well with the study by Piao et al. (2011) (SGS ranging from 120 to 170) and Che et al. (2014) (EGS ranging from 240 to 280), respectively, suggesting that SGS and EGS have different variation ranges on the TP. SGS ($R^2 = 0.77$, $p < 0.001$), GPP_{max} ($R^2 = 0.93$, $p < 0.001$), and EGS ($R^2 = 0.74$, $p < 0.001$) all have a strong spatial correlation with annual GPP (Fig. S6), indicating the strong

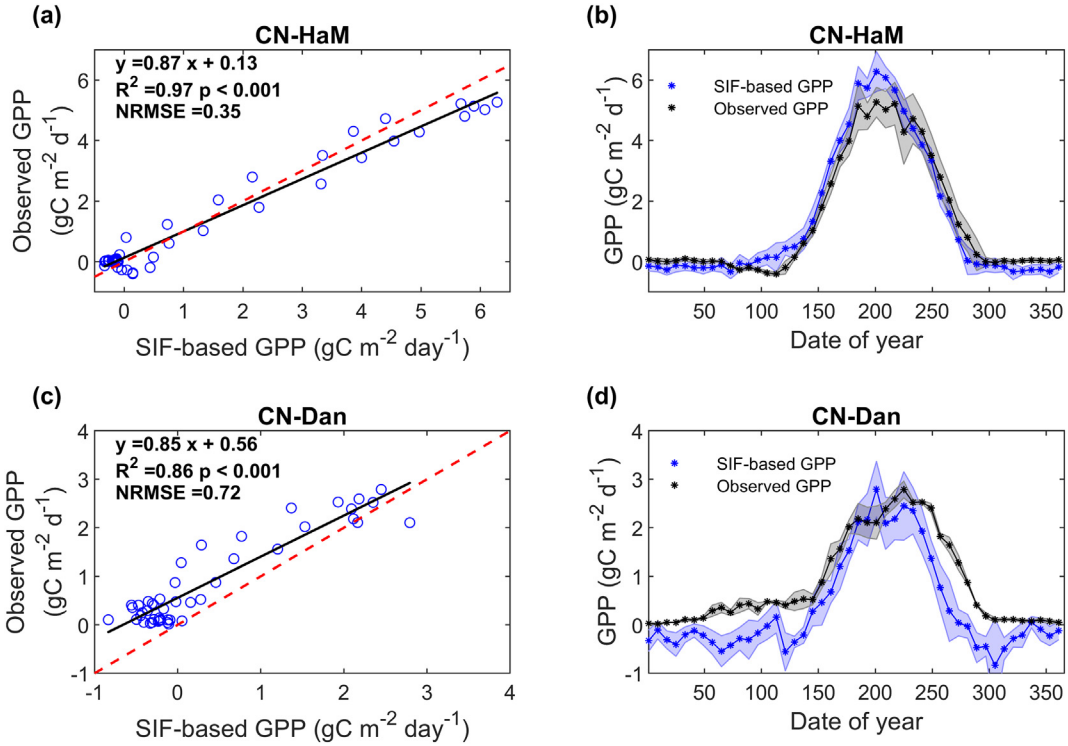

Fig. 4. Comparison of the SIF-based GPP with the observation GPP at two flux tower sites on the TP. Each dot indicates the multi-year averaged value at an 8-day interval. SIF-based GPP was averaged over 2007–2015 and flux GPP was averaged over the available period (2002–2004 for CN-HaM and 2004–2005 for CN-Dan). The shaded space indicates the 95% confidence intervals.

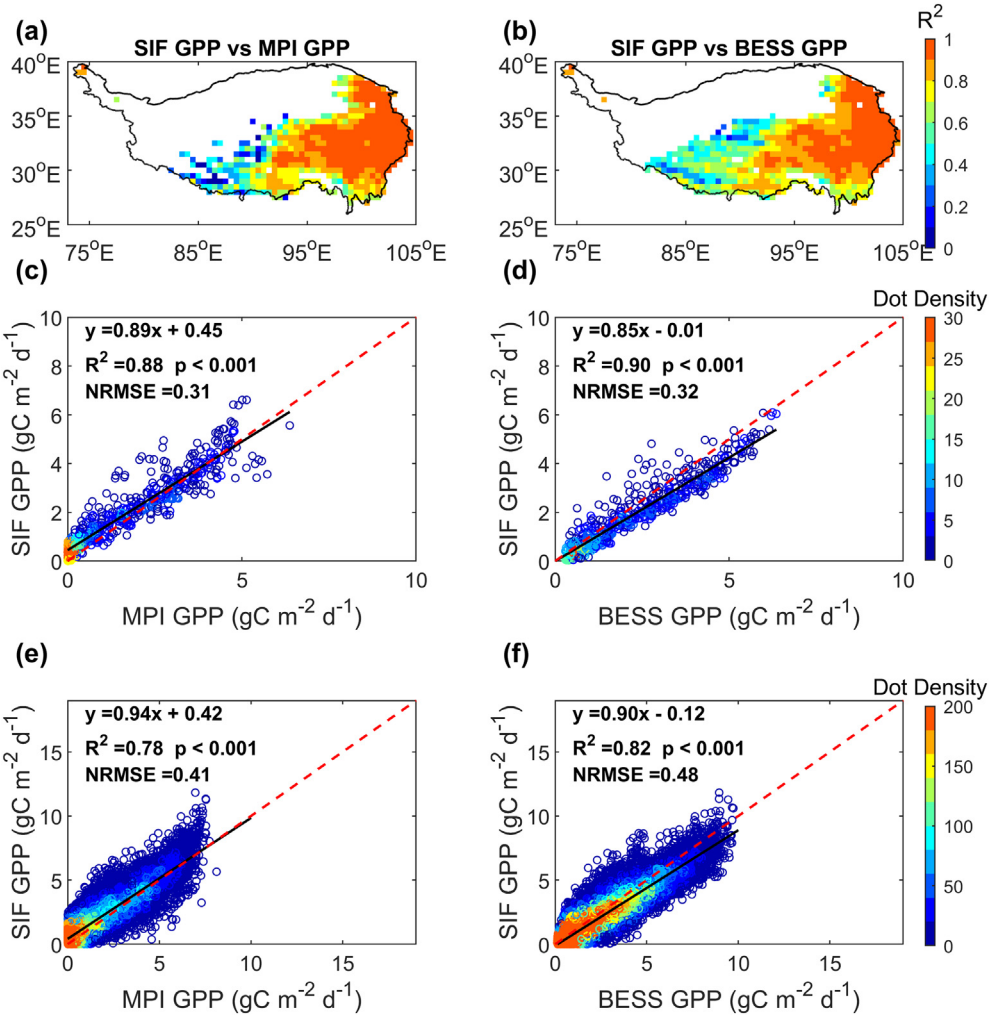

Fig. 5. Comparisons of the SIF-based GPP with MPI GPP and BESS GPP for temporal variability, spatial variability, and spatiotemporal variability, respectively. For temporal variability comparison, (a) and (b) show the spatial distribution of R^2 between the GPP time series for each pixel. For spatial variability comparison, each dot in (c) and (d) denotes the multi-year averaged value for each pixel. For spatiotemporal variability comparison, each dot in (e) and (f) denotes the monthly value for each pixel.

impact of phenology and physiology on the GPP spatial variations. The similar spatial patterns may be attributable to the spatial variation of climate conditions as both temperature and precipitation on the TP exhibit a decreasing gradient from southeast to northwest (Shen et al., 2011).

During 2007 to 2015, annual GPP in only 14.3% of the area shows significant trends, as the significant decreasing trends (-21.15 ± 9.72 gC m^{-2} $year^{-1}$, 11.2% of the area) and increasing trends (-8.43 ± 2.78 gC m^{-2} $year^{-1}$, only 3.1% of the area) primarily occur in the southeast and northwest, respectively (Fig. S7). Meanwhile, the three indicators exhibit significant change only in a small area during the study period, most of which were negative trends. SGS, GPP_{max}, and EGS have significant decreasing trends in 3.4%, 6.6%, and 5.4% of the area, with the trends at -3.87 ± 1.79 day $year^{-1}$, -0.24 ± 0.08 gC m^{-2} day^{-1}, and -2.47 ± 1.14 day $year^{-1}$, respectively (Fig. S7).

3.4. Quantifying the impact of phenological and physiological change on GPP

We firstly calculated the correlation coefficient (r) and sensitivity coefficient to estimate the impacts of phenological and physiological change on the corresponding seasonal carbon uptake (Keenan et al., 2014) based on the following simple regression model:

$$\Delta GPP_i = \alpha \Delta Indicator_i + \beta \quad (10)$$

where i denotes different indicators (i = SGS, GPP_{max}, and EGS) and GPP_i denotes their corresponding seasonal GPP (i.e., spring GPP, summer GPP, and autumn GPP, respectively), and the regression slope α refers to the sensitivity coefficient for quantifying the sensitivity of GPP_i to the variation of indicator i. Here, spring, summer, and autumn correspond to March to May, June to August, and September to November, respectively.

All of the indicators exhibit positive correlation with corresponding seasonal GPP across nearly the whole region ($r > 0$ in 84.3%, 97.2%, and 92.9% of the area, respectively, as shown in Fig. 7), indicating that advanced SGS, increasing GPP_{max}, and delayed EGS can all enhance corresponding seasonal carbon uptake. Specifically, GPP_{max} versus summer GPP demonstrates the strongest positive correlation ($r = 0.62 \pm 0.21$) with a sensitivity value of summer GPP to GPP_{max} of 42.5 ± 17.6 (Fig. 7a, b). In contrast, SGS versus spring GPP ($r = 0.49 \pm 0.24$) and EGS versus autumn GPP ($r = 0.54 \pm 0.23$) have a weaker but comparatively strong correlation (Fig. 7c, e). Moreover, the sensitivity of autumn GPP to EGS (2.46 gC m^{-2} d^{-1}) is slightly higher than the sensitivity of spring GPP to SGS (2.18 gC m^{-2} d^{-1}) but both share a somewhat similar spatial gradient descent from east to west (Fig. 7b, f).

The impacts of the three indicators on inter-annual GPP variability were further quantified with the developed multiple regression model (Eq. (9)). Since this model employs a key assumption that the three indicators are independent from each other, the inter-correlation of the three indicators was first tested. The results indicated that there was a

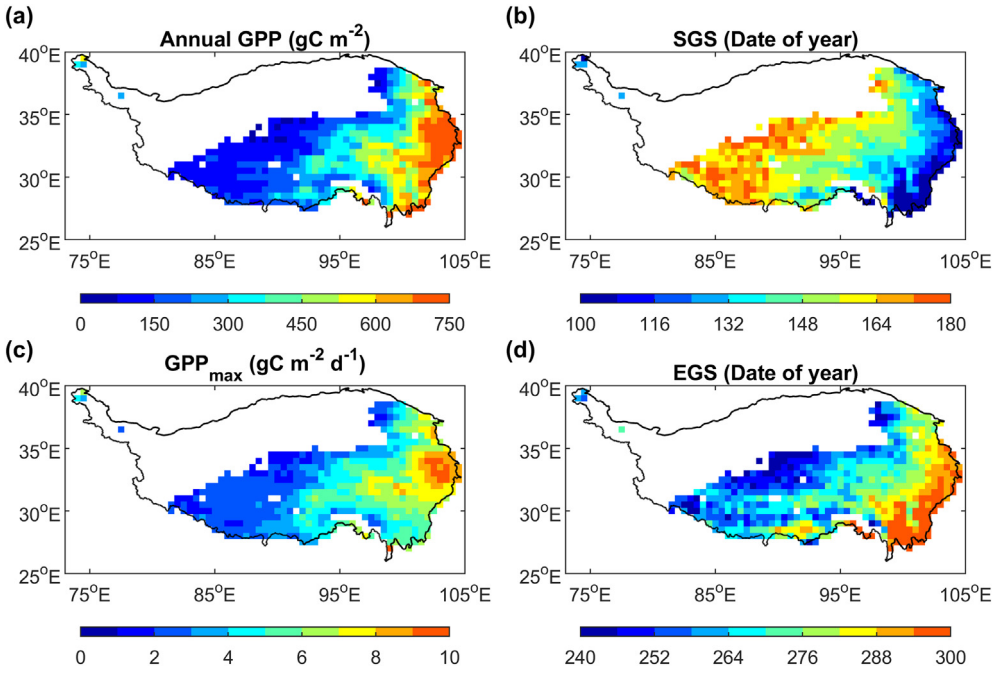

Fig. 6. Spatial distribution of the multi-year average of (a) annual GPP, (b) start date of the growing season (SGS), (c) maximum daily GPP (GPP_{max}), and (d) end date of the growing season (EGS) from 2007 to 2015 on the Tibetan Plateau.

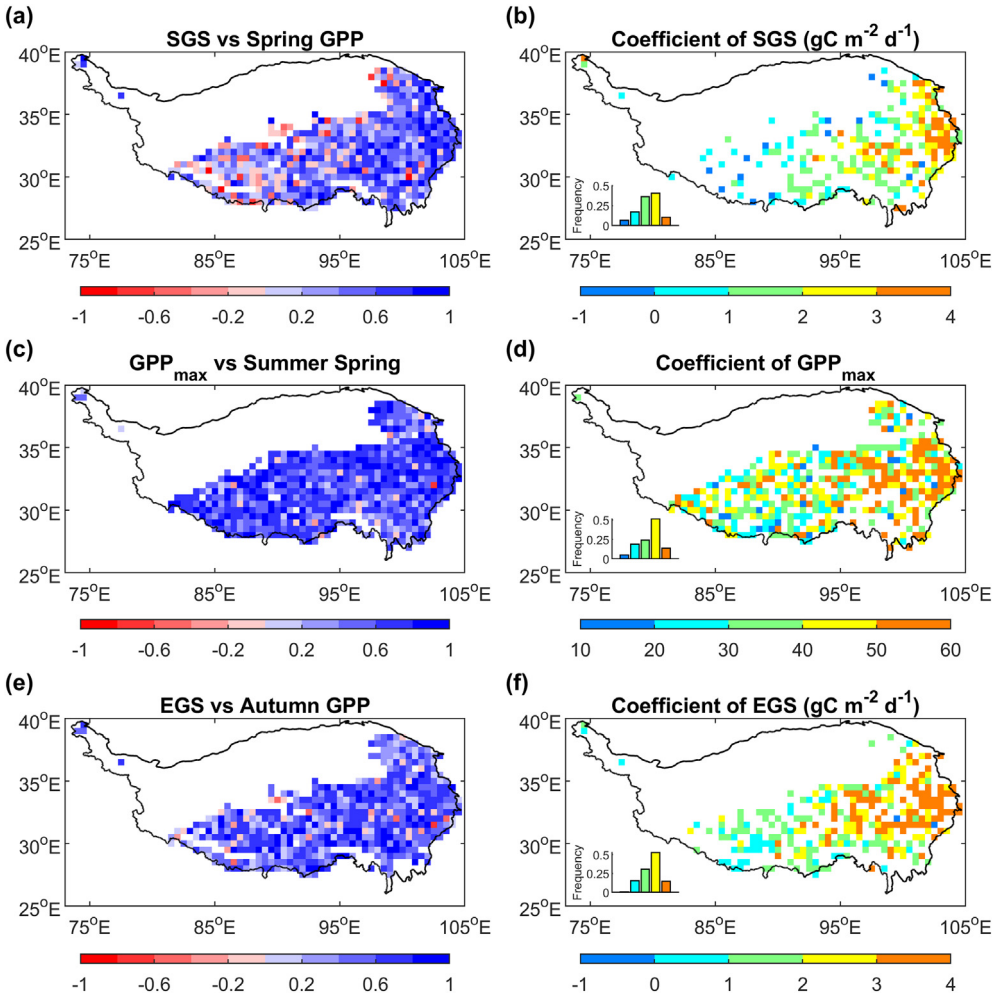

Fig. 7. Relationship between the seasonal GPP and corresponding phenological/physiological indicators from 2007 to 2015 over the Tibetan Plateau, namely the correlation coefficient (left part) and sensitivity coefficient (i.e., regression slope estimated based on Eq. (10), only the pixels with $p < 0.05$ retained, right part) for SGS versus spring GPP (March to May, (a) and (b)), GPP_{max} versus summer GPP (June to August, (c) and (d)) and EGS versus autumn GPP (September to November, (e) and (f)). Here, 365-SGS instead of SGS was used to make the sensitivity coefficients generated for SGS and EGS comparable.

weak correlation between the indicators, as only 4.2%, 6.7%, and 5.7% of area exhibits significance correlation ($p < 0.05$) for SGS versus GPP_{max}, SGS versus EGS, and EGS versus GPP_{max}, respectively, and the area proportion of pixels with absolute or <0.4 were 71.7%, 63.6% and 63.6%, respectively (Fig. S4). This suggests that the three indicators can reasonably be assumed to be independent of each other on the TP. Thus, the regression model was applied and demonstrated good performance in explaining the inter-annual GPP variability on the TP, with $R^2 = 0.72 \pm 0.20$ across the region (Fig. 8a). The annual GPP presents a positive response to increasing GPP_{max}, advanced SGS, and delayed EGS in the majority of the region (96.6%, 82.5%, and 84.7% of the area, respectively). The decline of GPP_{max} can considerably reduce carbon uptake on the TP, as a 1 gC m^{-2} day^{-1} decrease in GPP_{max} can yield a 37.15 ± 18.40 gC m^{-2} decrease in annual GPP (Fig. 8c). Meanwhile, annual GPP has a similar positive sensitivity to SGS and EGS, with 2.13 ± 2.17 and 2.51 ± 2.17 gC m^{-2} day^{-1}, respectively (Fig. 8b, d).

Furthermore, the relative contribution of each indicator to GPP inter-annual variability was determined through ANOVA analysis based upon the developed regression model. Clearly, GPP_{max} made the largest contribution to inter-annual GPP variability among the three indicators, with the GPP_{max} decline making a negative contribution of $-38.1 \pm 22.5\%$ in most areas (72.4%, Fig. 9b). However, the contribution of SGS and EGS shows great spatial heterogeneity. The positive contribution ($13.2 \pm 14.0\%$) from advanced SGS was primarily observed in the central and western region (53.4% of the total area), while the delayed SGS contributed negatively ($14.0 \pm 15.3\%$) mainly in the east (Fig. 9a). The advanced EGS that occurred in most areas led to a negative contribution ($-19.2 \pm 16.8\%$) in large parts of the TP (63.3%), while the delayed EGS made a positive contribution ($15.1 \pm 15.5\%$, Fig. 9c) in the remaining section of the region.

Hence, due to the negative contribution from both GPP_{max} decline and advanced EGS, annual GPP exhibited decreasing trends in the central and eastern part of the TP (Fig.S7a). Meanwhile, the increasing trend of annual GPP in the west is attributable to the positive contribution from the advanced SGS, which offset the negative contribution from the decline in GPP_{max}. The much larger contribution from GPP_{max} change than from SGS and EGS change indicates the greater importance

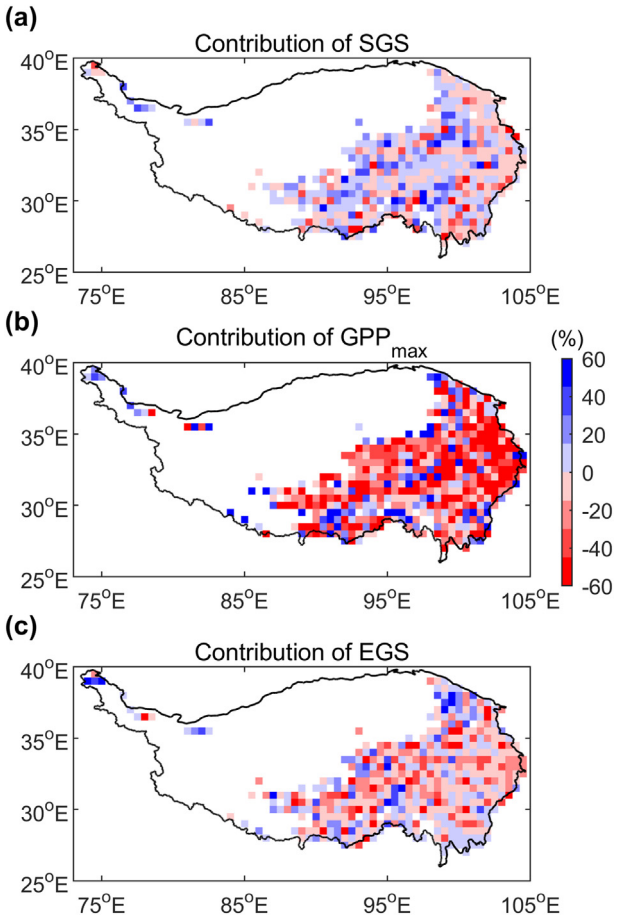

Fig. 9. Relative contribution of (a) SGS, (b) GPP_{max}, and (c) EGS to the inter-annual GPP variability during 2007 to 2015 on the Tibetan Plateau based on ANOVA analysis using the developed multiple regression model (Eq. (9)). Positive contribution indicates the change of the phenological/physiological indicator increase annual GPP and vice versa.

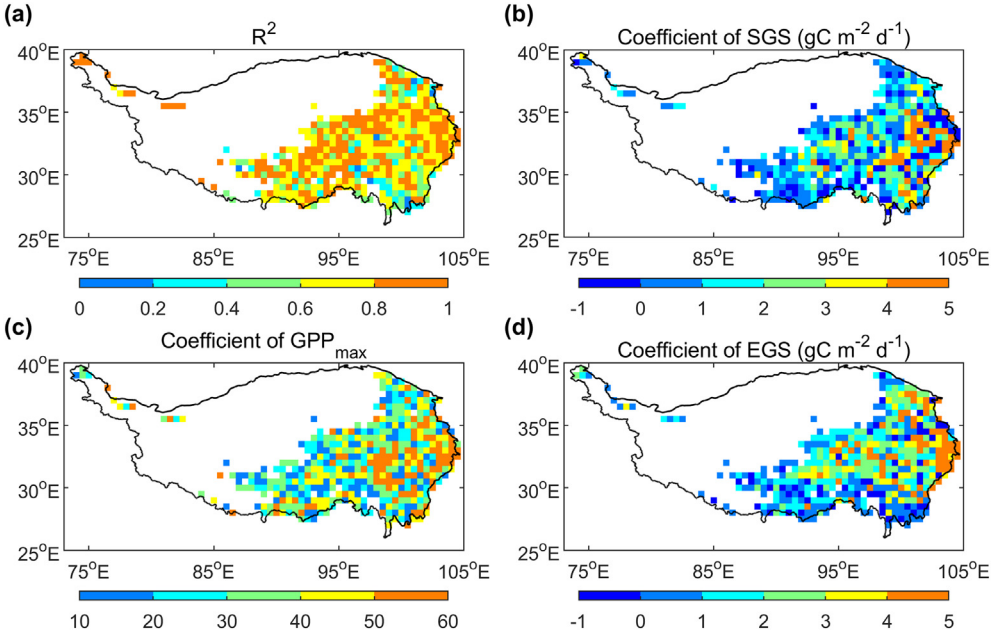

Fig. 8. Results of the multiple regression model with SGS, GPP_{max}, and ESG assembled (Eq. (9)) to explain GPP inter-annual variability from 2007 to 2015 on the Tibetan Plateau. Only pixels with $p < 0.5$ were retained and (a) shows the R^2 for the regression model. The sensitivity coefficients of annual GPP to (b) SGS, (c) GPP_{max}, and (d) EGS were estimated. Here, 365-SGS instead of SGS was used to make the sensitivity coefficients generated for SGS and EGS comparable.

of physiology to plant carbon uptake on the TP. We further evaluated the contribution differences of the three indicators to the inter-annual GPP variability among the different biomes. The results suggest that annual GPP variability is dominated by physiological change regardless of the biome type (Fig. S9).

3.5. Altitude dependence

There is great spatial variation in altitude on the TP, ranging from 3000 m to 5500 m (Fig. S1a). The influence of altitude on GPP and phenological metrics has been reported previously (Piao et al., 2011; Wang et al., 2017). Thus, the distribution of multi-year averaged annual GPP and three indicators across the variant altitude were investigated, with an altitude interval of 100 m. As shown in Fig.S10, with an increase in altitude, SGS advanced significantly at 0.026 day m^{-1} ($R^2 = 0.93$, $p < 0.001$), while EGS was significantly delayed at 0.017 day m^{-1} ($R^2 = 0.92$, $p < 0.001$). Meanwhile, both annual GPP ($R^2 = 0.93$, $p < 0.001$) and GPP_{max} ($R^2 = 0.93$, $p < 0.001$) decreased substantially with increasing altitude at a rate of −0.259 gC m^{-2} and –0.002 gC m^{-2} day^{-1} per m, respectively.

Whether the response of GPP to the three indicators varies with altitude was further investigated by analyzing the relationships between the sensitivity coefficients and the contributions of the three indicators to GPP and altitude. Here, we used the absolute value of sensitivity coefficients and the relative contributions to calculate the average at each altitude interval, thus neglecting the response direction. Moreover, as grassland (mainly distributed from 3500 m to 5000 m in altitude) accounts for approximately 90% of the vegetation cover in this region (Fig. 2) and FOR and SAS only cover areas with a small altitude range, we focused on the pixel dominated by GRA (fraction >60%) to exclude the influence from the differences in biomes. As shown in Fig. 10, all sensitivities of annual GPP to the three indicators significantly decreased as the altitude increased ($R^2 = 0.82$, $p < 0.001$ for SGS; $R^2 = 0.70$, $p < 0.001$ for GPP_{max}; and $R^2 = 0.90$, $p < 0.001$ for EGS). In contrast, along with the increasing altitude, the contribution of phenology to inter-annual GPP variability increased ($R^2 = 0.40$, $p = 0.01$ for SGS;

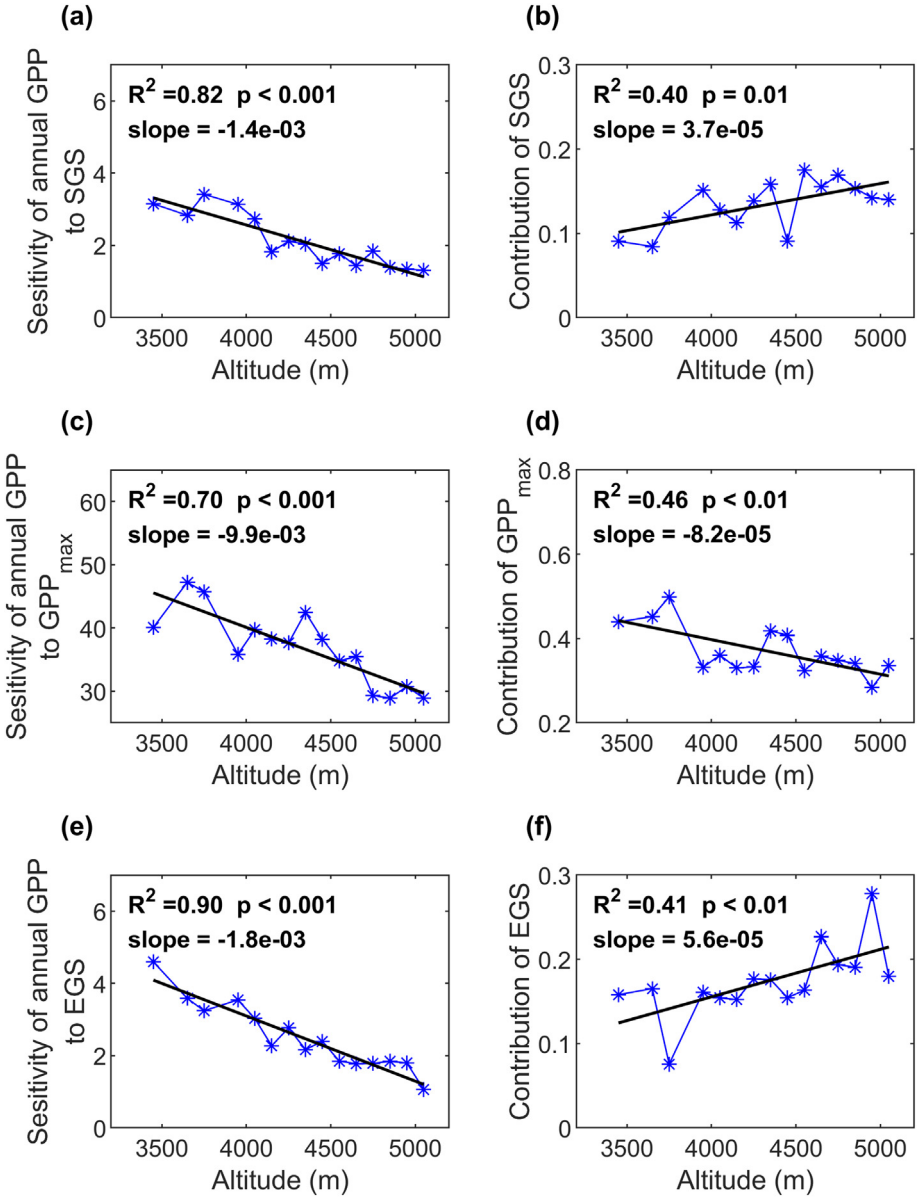

Fig. 10. The sensitivity coefficients of annual GPP to the three indicators (left part) and the relative contributions of the three indicators to annual GPP (right part) vary with altitude. The scatter plots indicated the mean value at an altitude interval of 100 m. Only the pixels with a land use fraction of grassland >60% were retained.

and $R^2 = 0.41$, $p < 0.01$ for EGS) while the contribution of physiology decreased ($R^2 = 0.46$, $p < 0.01$).

4. Discussion

4.1. Performance of the SIF-based GPP estimation and its implications

SIF space observations could provide the opportunity to continuously monitor the carbon flux for regions that lack ground observations with the simple method that was improved upon in this study. Compared to previous methods that neglect to consider the different components of vegetation in one SIF pixel (Guanter et al., 2014), we applied different SIF-GPP relationships for different biomes to map the spatially explicit GPP with the area fraction of each biome type considered in the calculation. We also validated the potential for using site observations from similar environments to estimate the SIF-GPP relationship in a region that lacks ground observations. With the SIF-GPP linear scaling estimated, the GOME-2 SIF retrievals can be scaled into GPP with an 8-day interval and 0.5° resolution based on the MODIS land cover data. Though mechanism models of inverting SIF to GPP (e.g., the SCOPE model) have been developed, they require vast amounts of input data for parameterization (Guan et al., 2016; Zhang et al., 2014). Thus, their application is constrained by the lack of ground observations for the TP. In comparison, though our approach is based simply on an empirical SIF-GPP relationship, it is feasible for this region and its estimation agrees well with flux observations and other estimation approaches, suggesting that we can obtain a satisfactory SIF-based GPP through the method proposed in this study.

GPP estimation based on both process-based models and data-oriented models requires a large number of local ground observations, and thus, the pronounced lack of ground observations on the TP leads to the great uncertainty in model simulation (Gao et al., 2014; Zhang et al., 2008). However, SIF-based estimation utilizes SIF space observations and site observations outside the region to obtain strong GPP estimation to overcome this obstacle. Furthermore, as mapping spatially explicit GPP with algorithms or parameters inferred at site level is inherently constrained by the TP's high spatial heterogeneity (Li et al., 2007; Piao et al., 2011), our SIF-based GPP estimation can provide a valuable independent data source to constrain the parameterizations, thus improving the accuracy of the model simulation of this region (Guan et al., 2017; Joiner et al., 2014).

Carbon assimilation in the TP, the largest alpine ecosystem in the world, has a vital role in the global carbon balance (Kato et al., 2004; Zhuang et al., 2010). As the importance of ecological conservation of the TP has become widely acknowledged, national nature reserves have been established and protection programs have been implemented in the region (Chen et al., 2014; Chen et al., 2013). Hence, SIF-based GPP monitoring can provide continuous feedback for the ecological management of the TP and valuable information for the global carbon balance. With ongoing development of spectral technology and newly launched satellites (i.e., Orbiting Carbon Observatory-2 (OCO-2) and Sentinel-5 Precursor), improved SIF space measurements at higher spatial or temporal resolution are expected to be obtained in the near future (Guan et al., 2016), providing a promising opportunity for enhanced GPP estimation.

4.2. Impact of phenology and physiology on carbon uptake

Our study demonstrates that carbon uptake on the TP is determined by phenology and photosynthesis physiology, as the proposed model incorporating SGS, GPP_{max}, and EGS interprets 72 ± 20% of inter-annual GPP variability (Xia et al., 2015). Furthermore, our study suggests that physiology dominates the carbon uptake in most areas of the TP, consistent with previous studies conducted on North America (Xia et al., 2015; Zhou et al., 2017). Advanced SGS and delayed EGS, which can both extend CUP, significantly enhanced spring or autumn carbon uptake on the TP. However, photosynthesis in both spring and autumn was constrained by the low temperatures on the TP, causing the daily GPP in both seasons to be much smaller than that in summer. Thus, the annual carbon uptake is mainly determined by summer GPP and is primarily attributable to GPP_{max} as opposed to SGS or EGS. Given the importance of GPP_{max} for carbon uptake on the TP, we suggest that more attention should be given to the mechanism of physiological change in the alpine ecosystem to potentially enhance GPP estimation and projection.

It was found that the response of GPP to phenology and physiology on the TP has significant altitude dependence. As altitude increases, the annual temperature and the available nutrition decline (Korner, 2007), constraining summer photosynthesis capacity (i.e., GPP_{max}). Hence, spring and autumn GPP accounts for a larger proportion of annual GPP with increasing altitude and annual GPP for high altitude areas can be increased considerably by CUP extension. As a result, the contribution of physiology to inter-annual GPP variability decreases as altitude increases and phenological change becomes the dominant factor of annual GPP variability in high altitude areas. Additionally, the response of phenology and physiology to climate variations on the TP also has an altitude dependency (Piao et al., 2011). Because of the high spatial variation of altitude on the TP, altitude dependency should be considered in relevant ecological models and future GPP projection.

To our knowledge, our study is the first to quantitatively separate the contributions of phenological and physiological change to inter-annual GPP variability on the TP and assess the altitude independence of these contributions. As previous works have primarily focused on the mechanism of phenological change on the TP (Shen et al., 2016; Shen et al., 2015; Yang et al., 2017), our study of GPP_{max} (an indicator of photosynthesis capacity) can fill the gap on physiological study in this region (Fu et al., 2015). More importantly, our study has revealed how these climate-induced phenological and physiological changes have affected carbon uptake in the region, thus revealing the underlying mechanism of GPP variability and providing a better theoretical foundation for future GPP modeling in the TP region.

4.3. Role of climate variations on the response of GPP to phenology and physiology

The analysis results above revealed the significant contribution of phenological and physiological change on the GPP spatiotemporal variability on the TP. How do climate variations on the TP affect the response of GPP to phenological and physiological indicators? Vegetation activities are primarily affected by three climate factors: temperature, water availability, and solar radiation (Nemani et al., 2003). The TP region possesses enough solar radiation (Zhao et al., 2006) that the vegetation is insensitive to it (Cong et al., 2016). Hence, we only tested the partial correlation between the three indicators and their preseason temperature and precipitation. For each pixel, the preseason was considered to be the 30 days before the multi-year averaged DOY of the metrics.

Overall, in Fig. 11, all three indicators presented strong partial correlation with both preseason temperature and precipitation but displayed opposite responses to preseason climate variations in different areas. SGS exhibited strong positive correlation ($r = 0.44 \pm 0.23$) with preseason temperature in 55.5% of the area (12.5% of which had a significance level of $p < 0.05$), mainly located in the central and mid-western part of the region, while SGS in the other part had a strong negative correlation ($r = -0.43 \pm 0.23$) with preseason temperature. Thus, the warming trend could delay or advance SGS in the TP. Consistently, different studies have found opposite SGS responses to the warming trend in this region (Shen et al., 2015; Yu et al., 2010; Zheng et al., 2016). Meanwhile, EGS showed strong positive correlation ($r = 0.43 \pm 0.23$) with preseason temperature in the majority of the region (66.7%)—consistent with the work by Cong et al. (2016). As negative correlations ($r = -0.40 \pm 0.22$) between EGS and preseason temperature were observed in the

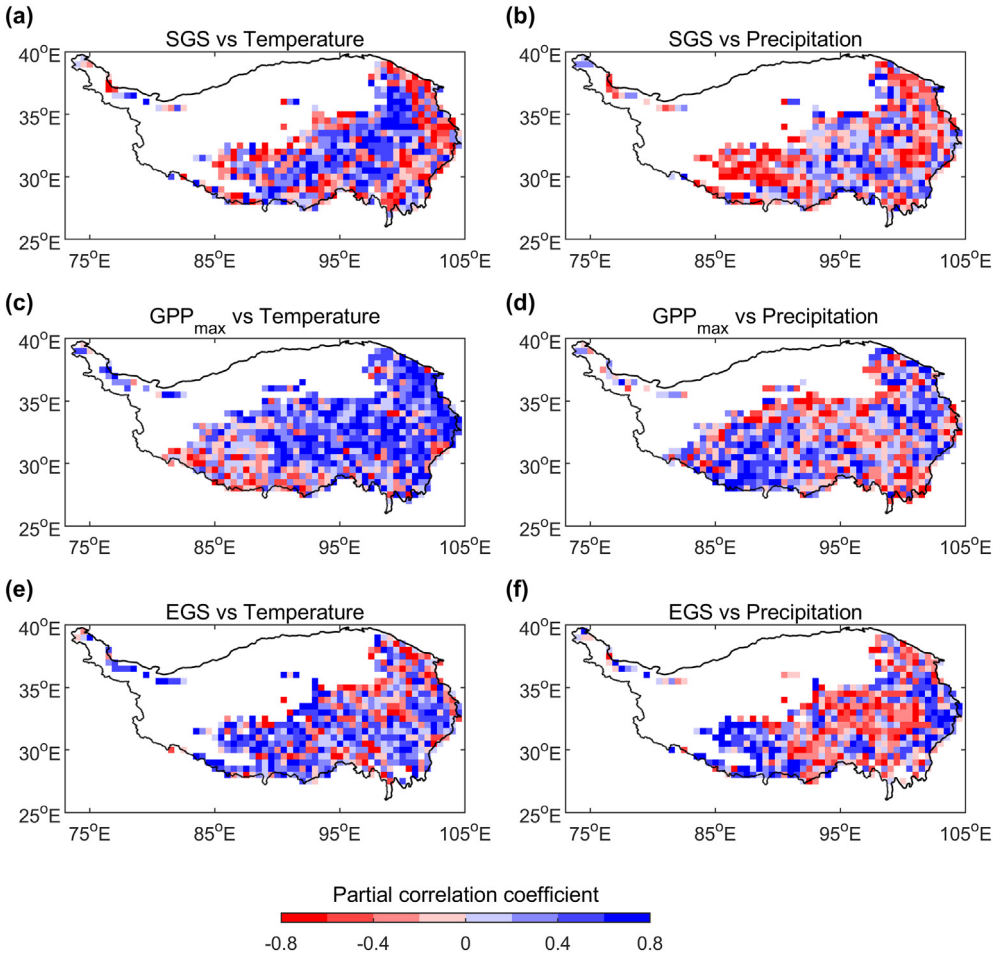

Fig. 11. Partial correlation between three indicators and preseason temperature (with precipitation controlled, left side) or precipitation (with temperature controlled, right side). Preseason is defined as 30 days before the mean date of the phenological/physiological indicator.

left area, we further assessed the impact of growing season temperature on EGS. However, their correlation is roughly similar to that between preseason temperature and EGS (Fig.S12), suggesting that more research is needed to investigate the mechanism of EGS variations. Increasing precipitation could advance SGS ($r = -0.41 \pm 0.25$) and delay EGS ($r = 0.44 \pm 0.24$) in half of the region, distributed in the east and west of the TP. For most of the area, GPP_{max} was strongly correlated with both preseason temperature ($r = 0.45 \pm 0.23$, 73.8% of the TP) and precipitation ($r = 0.39 \pm 0.24$, 58.1% of the TP), of which 16.5% and 11.7% were significant ($p < 0.05$), respectively.

As different areas of the TP have distinct geographies, climatic conditions, and diverse vegetation communities, the huge amount of spatial heterogeneity could induce vegetation to exhibit different responses to climate change (Chen et al., 2013). Therefore, in contrast to the relatively consistent response to temperature in other regions (Zhou et al., 2017), significant spatial variations of magnitude or even direction for phenology responding to climate change have been observed on the TP (Cong et al., 2016; Shen et al., 2011), which is consistent with our results. As shown in Fig.S13, different biomes have distinctly different responses to both preseason temperature and precipitation (different variation ranges of partial correlation coefficients), indicating that the diverse vegetation components in this region may contribute to the spatial heterogeneity of the three indicators' responses to climate variations (Shen et al., 2015). Conversely, since the TP is characterized by a cold and arid or semiarid environment, both temperature and water availability are the critical factors regulating vegetation phenology and physiology (Shen et al., 2011). Thus, the response of vegetation to climate change depends on its local climatic background (Shen et al., 2011; Shen et al., 2015). For example, spring warming tends to advance SGS in relatively wetter areas, while increasing precipitation has a greater impact on phenology in drier areas (Cong et al., 2016, Shen et al., 2011). As the TP has huge spatial variations in climatic background (i.e., different water-energy conditions, as shown in Fig. S1), vegetation phenology and physiology are expected to have different spatial responses to climate change. Furthermore, this great spatial variation might be attributable to a complicated underlying mechanism. Though spring warming can lead to earlier spring phenology (Piao et al., 2011; Zhang et al., 2013), winter warming on the TP could slow the fulfillment of the chilling requirement, thus delaying the spring phenology (Yu et al., 2010).

Given the rate of projected climate change, climate-induced changes in vegetation phenology and physiology are likely to continuously alter carbon balance on the TP. As GPP_{max} is dominated by temperature as opposed to precipitation in most areas of the TP, the projected temperature increases (IPCC, 2007; Piao et al., 2011) have the potential to raise the GPP_{max} in most areas, thus increasing annual GPP. Physiological change in vegetation, induced by extreme climate events such as summer droughts, can considerably reduce GPP (Zhou et al., 2017). Hence, an increasing frequency of extreme climate events on the TP (Xi et al., 2018), along with huge uncertainty in the projected precipitation (Lu et al., 2018), will lead to significant uncertainty with regard to GPP variability and pose risks for future ecological conservation. Furthermore, as the carbon cycle couples with the water cycle (Beer et al., 2010; Piao et al., 2009), variation in GPP can influence the water consumed by vegetation, thus affecting the runoff generated (Zhang et al., 2011). Increasing runoff induced by physiological change over the past few

decades has been detected (Betts et al., 2007). As the TP is the source region for the three largest rivers in China, evaluating the runoff change induced by GPP variability is imperative.

4.4. Limitations and uncertainties of the results

The limitations and uncertainties of the results of our study primarily stem from the data and methodology used. Our study was highly dependent on the quality of the GOME-2 SIF datasets, which can be affected by the measurement instruments, algorithms, and sky conditions (Joiner et al., 2013; Köhler et al., 2015; Shen et al., 2015). The SIF dataset that was used is a new version developed by Köhler et al. (2015) and its retrieval windows and algorithms are different from the version employed by Joiner et al. (2013). Though different versions have a discrepancy in absolute values, their spatiotemporal pattern is highly consistent (Köhler et al., 2015). As the SIF is linearly scaled into GPP, the version of data used has no impact on the GPP estimation. Although the SIF data quality was moderately influenced by clouds, the impact of clouds has been minimized because the measurements with a cloud fraction larger than 0.5 were excluded (Köhler et al., 2015). Furthermore, the TP is a region with few clouds, naturally reducing this type of uncertainty. Since previous studies have reported the minimal impact of sun-view geometry variations on the SIF space observations (He et al., 2017) and the variations of sun-view geometry induced by altitude differences are more limited, the unwanted uncertainties of SIF observations induced by altitude variations on the TP are expected to have less of an impact on our results and conclusions. However, this still warrants further investigation in future research. Though the GOME-2 SIF was measured at approximately 9:30 a.m. locally, it shows high consistency with the simulated SIF (9:00–12:00 a.m.) based on a mechanism model (Zhang et al., 2014). Given the influence of the midday peak value on the diurnal photosynthesis cycle (Katul et al., 2009), this consistency suggests that it is representative of photosynthesis conditions on a daily scale. However, the discrepancy between the instantaneous sample and diurnal cycle should be noted and our averaging of individual retrievals into 8-day intervals can reduce the uncertainties to some extent.

Besides the SIF dataset, the uncertainties of our GPP estimation also depend on our estimation approach. We have noted that the SIF-GPP relationship differs slightly at different sites, even those with the same biome type and a similar environment, which indicates that applying an empirically universal SIF-GPP linear scaling for each biome would introduce uncertainties into GPP estimation. However, the difference in the SIF-GPP relationship between different sites of the same biome is relatively small (Fig. S2), and the statistical significance indicates that a universal SIF-GPP scaling can be trusted and is acceptable. The uncertainties primarily influence the GPP magnitude, which is quantified with 95% confidence intervals (Fig. S5) and we found that the relative uncertainty range is small at 6.5%. Furthermore, the magnitude of our SIF-based GPP has high consistency with both MPI and BESS GPP (Fig. 5), indicating that a satisfactory GPP estimation can be obtained through this method. Conversely, the spatial variation within a SIF pixel would introduce uncertainty into the estimated SIF-GPP relationship, though we applied homogeneity criteria to screen the sites. Though the OCO-2 SIF data is limited in its narrow swaths, its similar footprint (1.5×2.3 km) to flux sites can provide a better estimated SIF-GPP relationship in future research (Sun et al., 2017).

In terms of the derived phenological and physiological metrics, the uncertainties are related to the capacity of SIF to capture the seasonal cycle as well as the approach used to derive the metrics. As the original SIF retrievals are directly and linearly scaled into GPP, the estimated SIF-GPP relationship has little impact on the derived phenological indicators. As shown in Fig. S14, both SGS ($R^2 = 0.99$, NRMSE = 0.02) and EGS ($R^2 = 0.99$, NRMSE = 0.01) derived from the original SIF and SIF-derived GPP show a high consistency. Many approaches have been developed to derive phenological and physiological metrics. However, previous studies have found that different methods would affect the specific DOY of the derived SGS and EGS, but would have less impact on the trend of their DOY (Cong et al., 2012). As our quantitative analysis was based on the inter-annual variation of phenological and physiological indicators instead of their absolute value, the method used has little impact on our results. To avoid system bias, two widely validated methods were applied to derive phenological and physiological metrics and found that the results generated by two independent methods coincided with each other.

The accuracy of the SIF seasonal dynamics has significant impact on the derived phenological and physiological indicators and the relevant results. The ability of GOME-2 SIF in tracking the photosynthesis seasonal cycle has been well validated in many regions (Guanter et al., 2014; Joiner et al., 2014), but has not been previously assessed in the TP region. Though we lacked sufficient ground observations for further evaluation in this region, the earlier slight drop of SIF at the CN-Dan site and the weak correlation with BESS and MPI GPP in some pixels in the west part of the TP should be noted. As EVI is widely used as a vegetation index for investigating vegetation seasonality on the TP (Shen et al., 2015), we further compared the performance of GOME-2 SIF and MODIS EVI to capture seasonality at two grassland sites on the TP. As the flux record has no overlap with the period of SIF, we compared their multi-year averaged seasonal curves. Both SIF and EVI have comparably high performance at the CN-HaM site while EVI ($R^2 = 0.98$) does slightly better than SIF ($R^2 = 0.91$) at the CN-Dan site (Fig. S15). However, we found it difficult to identify the absence of vegetation photosynthesis with the reflectance-based EVI as its minimum values rely on the soil background or snow (Guanter et al., 2014, Joiner et al., 2014). In contrast, as a direct signal of vegetation photosynthesis, the SIF drops to be zero to avoid being ambiguous, reflecting that it has a more inherent relation to GPP than EVI. Consistent with our study, many studies have reported the differences in vegetation dynamics inferred from various satellite-based or model-based products (Joiner et al., 2014), suggesting that more ground observation is required for enhanced evaluation and validation.

5. Conclusions

This study explored the potential of GPP estimation based on SIF space observations and our improved approach, and quantitatively separated the impact of phenology and physiology on inter-annual GPP variability in the TP region. The obtained SIF-based GPP agreed well with flux observations and two state of the art GPP products, with regional carbon uptake values of 0.62 ± 0.04 PgC year^{-1} or 307 ± 22 gC m^{-2} year^{-1}. Both phenology (SGS and ESG) and physiology (GPP_{max}) have great impact on seasonal and annual GPP spatiotemporal variability and together can explain $72 \pm 20\%$ of GPP inter-annual variability. However, physiology has a much larger contribution to inter-annual GPP variability than that of phenology in most areas of the TP. The response of annual GPP to phenological and physiological change has a significant altitude dependence, as the contribution of physiology to annual carbon uptake decreased with increasing altitude and phenology dominated in high altitude areas. As a result, during 2007–2015, the decline in annual GPP in the western region of the TP was primarily attributable to the decrease in the GPP_{max}, while the increase in annual GPP in the east is attributable to the advanced SGS. With the additional analysis, we found that the response of phenology and physiology to both temperature and precipitation variation has strong spatial heterogeneity, which may be attributable to the huge spatial variations of both local biomes and climate background in this region. Our study demonstrates that the satellite-based SIF dataset combined with our improved approach can provide outstanding GPP estimation in a region that lacks ground observations. Our better understanding of the impact of climate-induced phenological and physiological change on GPP variability in alpine ecosystems can improve GPP estimation and ecological environmental assessment in a changing climate.

Acknowledgments

This study was financially supported by the National Natural Science Foundation of China (No.91647212) and by the National Key Research and Development Program of China (2016YFE0201900 and 2017YFC0403600). We thank Min Chen for providing the MPI GPP products.

Appendix A. Supplementary data

Supplementary data to this article can be found online at https://doi.org/10.1016/j.scitotenv.2019.01.324.

References

Ballantyne, A.P., Alden, C.B., Miller, J.B., Tans, P.P., White, J.W.C., 2012. Increase in observed net carbon dioxide uptake by land and oceans during the past 50 years. Nature 488, 70.

Beer, C., Reichstein, M., Tomelleri, E., et al., 2010. Terrestrial gross carbon dioxide uptake: global distribution and covariation with climate. Science 329, 834–838.

Betts, R.A., Boucher, O., Collins, M., et al., 2007. Projected increase in continental runoff due to plant responses to increasing carbon dioxide. Nature 448, 1037.

Che, M., Chen, B., Innes, J.L., et al., 2014. Spatial and temporal variations in the end date of the vegetation growing season throughout the Qinghai–Tibetan Plateau from 1982 to 2011. Agric. For. Meteorol. 189, 81–90.

Chen, H., Zhu, Q.A., Peng, C.H., et al., 2013. The impacts of climate change and human activities on biogeochemical cycles on the Qinghai-Tibetan Plateau. Glob. Chang. Biol. 19, 2940–2955.

Chen, B.X., Zhang, X.Z., Tao, J., et al., 2014. The impact of climate change and anthropogenic activities on alpine grassland over the Qinghai-Tibet Plateau. Agric. For. Meteorol. 189, 11–18.

Collatz, G.J., Berry, J.A., Clark, J.S., 1998. Effects of climate and atmospheric CO_2 partial pressure on the global distribution of C4 grasses: present, past, and future. Oecologia 114, 441–454.

Cong, N., Piao, S.L., Chen, A.P., et al., 2012. Spring vegetation green-up date in China inferred from SPOT NDVI data: a multiple model analysis. Agric. For. Meteorol. 165, 104–113.

Cong, N., Shen, M., Piao, S., 2016. Spatial variations in responses of vegetation autumn phenology to climate change on the Tibetan Plateau. J. Plant Ecol. 10, 744–752.

Friedl, M.A., Mciver, D.K., Hodges, J.C., et al., 2002. Global land cover mapping from MODIS: algorithms and early results. Remote Sens. Environ. 83, 287–302.

Fu, G., Shen, Z.-X., Sun, W., Zhong, Z.-M., Zhang, X.-Z., Zhou, Y.-T., 2015. A meta-analysis of the effects of experimental warming on plant physiology and growth on the Tibetan Plateau. J. Plant Growth Regul. 34, 57–65.

Gao, Y.H., Zhou, X., Wang, Q., et al., 2013. Vegetation net primary productivity and its response to climate change during 2001–2008 in the Tibetan Plateau. Sci. Total Environ. 444, 356–362.

Gao, Y.N., Yu, G.R., Yan, H.M., et al., 2014. A MODIS-based photosynthetic capacity model to estimate gross primary production in Northern China and the Tibetan Plateau. Remote Sens. Environ. 148, 108–118.

Guan, K., Berry, J.A., Zhang, Y., Joiner, J., Guanter, L., Badgley, G., Lobell, D.B., 2016. Improving the monitoring of crop productivity using spaceborne solar-induced fluorescence. Glob. Chang. Biol. 22, 716–726.

Guan, K., Wu, J., Kimball, J.S., et al., 2017. The shared and unique values of optical, fluorescence, thermal and microwave satellite data for estimating large-scale crop yields. Remote Sens. Environ. 199, 333–349.

Guanter, L., Zhang, Y., Jung, M., et al., 2014. Global and time-resolved monitoring of crop photosynthesis with chlorophyll fluorescence. Proc. Natl. Acad. Sci. 111, E1327–E1333.

He, L., Chen, J.M., Liu, J., Mo, G., Joiner, J., 2017. Angular normalization of GOME-2 sun-induced chlorophyll fluorescence observation as a better proxy of vegetation productivity. Geophys. Res. Lett. 44, 5691–5699.

Hutchinson, M.F., 1998a. Interpolation of rainfall data with thin plate smoothing splines. Part I: two dimensional smoothing of data with short range correlation. J. Geogr. Inf. Decis. Anal. 2, 139–151.

Hutchinson, M.F., 1998b. Interpolation of rainfall data with thin plate smoothing splines. Part II: analysis of topographic dependence. J. Geogr. Inf. Decis. Anal. 2, 152–167.

IPCC, 2007. Climate change 2007: the physical science basis. Agenda 6, 333.

Jiang, C., Ryu, Y., 2016. Multi-scale evaluation of global gross primary productivity and evapotranspiration products derived from Breathing Earth System Simulator (BESS). Remote Sens. Environ. 186, 528–547.

Joiner, J., Guanter, L., Lindstrot, R., et al., 2013. Global monitoring of terrestrial chlorophyll fluorescence from moderate-spectral-resolution near-infrared satellite measurements: methodology, simulations, and application to GOME-2. Atmos. Meas. Tech. 6, 2803–2823.

Joiner, J., Yoshida, Y., Vasilkov, A., et al., 2014. The seasonal cycle of satellite chlorophyll fluorescence observations and its relationship to vegetation phenology and ecosystem atmosphere carbon exchange. Remote Sens. Environ. 152, 375–391.

Jung, M., Reichstein, M., Margolis, H.A., et al., 2011. Global patterns of land-atmosphere fluxes of carbon dioxide, latent heat, and sensible heat derived from eddy covariance, satellite, and meteorological observations. J. Geophys. Res. Biogeosci. 116.

Kato, T., Tang, Y.H., Gu, S., et al., 2004. Carbon dioxide exchange between the atmosphere and an alpine meadow ecosystem on the Qinghai-Tibetan Plateau, China. Agric. For. Meteorol. 124, 121–134.

Kato, T., Tang, Y.H., Gu, S., Hirota, M., Du, M.Y., Li, Y.N., Zhao, X.Q., 2006. Temperature and biomass influences on interannual changes in CO2 exchange in an alpine meadow on the Qinghai-Tibetan plateau. Glob. Chang. Biol. 12, 1285–1298.

Katul, G.G., Palmroth, S., Oren, R., 2009. Leaf stomatal responses to vapour pressure deficit under current and CO_2-enriched atmosphere explained by the economics of gas exchange. Plant Cell Environ. 32, 968–979.

Keenan, T.F., Gray, J., Friedl, M.A., et al., 2014. Net carbon uptake has increased through warming-induced changes in temperate forest phenology. Nat. Clim. Chang. 4, 598–604.

Köhler, P., Guanter, L., Joiner, J., 2015. A linear method for the retrieval of sun-induced chlorophyll fluorescence from GOME-2 and SCIAMACHY data. Atmos. Meas. Tech. 8, 2589.

Korner, C., 2007. The use of 'altitude' in ecological research. Trends Ecol. Evol. 22, 569–574.

Lee, J.-E., Frankenberg, C., Van Der Tol, C., et al., 2013. Forest productivity and water stress in Amazonia: observations from GOSAT chlorophyll fluorescence. Proc. R. Soc. Lond. B Biol. Sci. 280, 20130171.

Li, Z.Q., Yu, G.R., Xiao, X.M., et al., 2007. Modeling gross primary production of alpine ecosystems in the Tibetan Plateau using MODIS images and climate data. Remote Sens. Environ. 107, 510–519.

Li, H.Q., Zhang, F.W., Li, Y.N., et al., 2016. Seasonal and inter-annual variations in CO_2 fluxes over 10 years in an alpine shrubland on the Qinghai-Tibetan Plateau, China. Agric. For. Meteorol. 228, 95–103.

Lu, W., Wang, W., Shao, Q., et al., 2018. Hydrological projections of future climate change over the source region of Yellow River and Yangtze River in the Tibetan Plateau: a comprehensive assessment by coupling RegCM4 and VIC model. Hydrol. Process. 32, 2096–2117.

Monteith, J., 1972. Solar radiation and productivity in tropical ecosystems. J. Appl. Ecol. 9, 747–766.

Nemani, R.R., Keeling, C.D., Hashimoto, H., et al., 2003. Climate-driven increases in global terrestrial net primary production from 1982 to 1999. Science 300, 1560–1563.

Pan, Y., Birdsey, R.A., Fang, J., et al., 2011. A large and persistent carbon sink in the world's forests. Science 1201609.

Piao, S., Fang, J., Zhou, L., Ciais, P., Zhu, B., 2006. Variations in satellite-derived phenology in China's temperate vegetation. Glob. Chang. Biol. 12, 672–685.

Piao, S., Fang, J., Ciais, P., Peylin, P., Huang, Y., Sitch, S., Wang, T., 2009. The carbon balance of terrestrial ecosystems in China. Nature 458, 1009.

Piao, S.L., Cui, M.D., Chen, A.P., Wang, X.H., Ciais, P., Liu, J., Tang, Y.H., 2011. Altitude and temperature dependence of change in the spring vegetation green-up date from 1982 to 2006 in the Qinghai-Xizang Plateau. Agric. For. Meteorol. 151, 1599–1608.

Richardson, A.D., Hollinger, D.Y., Dail, D.B., Lee, J.T., Munger, J.W., O'keefe, J., 2009. Influence of spring phenology on seasonal and annual carbon balance in two contrasting New England forests. Tree Physiol. 29, 321–331.

Richardson, A.D., Black, T.A., Ciais, P., et al., 2010. Influence of spring and autumn phenological transitions on forest ecosystem productivity. Philos. Trans. R. Soc., B 365, 3227–3246.

Running, S.W., Thornton, P.E., Nemani, R., Glassy, J.M., 2000. Global terrestrial gross and net primary productivity from the earth observing system. Methods in Ecosystem Science. Springer.

Ryu, Y., Baldocchi, D.D., Kobayashi, H., et al., 2011. Integration of MODIS land and atmosphere products with a coupled-process model to estimate gross primary productivity and evapotranspiration from 1 km to global scales. Glob. Biogeochem. Cycles 25.

Shen, M., 2011. Spring phenology was not consistently related to winter warming on the Tibetan Plateau. Proc. Natl. Acad. Sci. 108, E91–E92.

Shen, M., Tang, Y., Chen, J., Zhu, X., Zheng, Y., 2011. Influences of temperature and precipitation before the growing season on spring phenology in grasslands of the central and eastern Qinghai-Tibetan Plateau. Agric. For. Meteorol. 151, 1711–1722.

Shen, M.G., Piao, S.L., Dorji, T., et al., 2015. Plant phenological responses to climate change on the Tibetan Plateau: research status and challenges. Nat. Sci. Rev. 2, 454–467.

Shen, M.G., Piao, S.L., Chen, X.Q., et al., 2016. Strong impacts of daily minimum temperature on the green-up date and summer greenness of the Tibetan Plateau. Glob. Chang. Biol. 22, 3057–3066.

Still, C.J., Berry, J.A., Collatz, G.J., Defries, R.S., 2003. Global distribution of C3 and C4 vegetation: carbon cycle implications. Glob. Biogeochem. Cycles 17.

Sun, Y., Frankenberg, C., Wood, J.D., et al., 2017. OCO-2 advances photosynthesis observation from space via solar-induced chlorophyll fluorescence. Science 358, eaam5747.

Wang, S.Y., Zhang, B., Yang, Q.C., et al., 2017. Responses of net primary productivity to phenological dynamics in the Tibetan Plateau, China. Agric. For. Meteorol. 232, 235–246.

White, M.A., De Beurs, K.M., Didan, K., et al., 2009. Intercomparison, interpretation, and assessment of spring phenology in North America estimated from remote sensing for 1982–2006. Glob. Chang. Biol. 15, 2335–2359.

Xi, Y., Miao, C., Wu, J., Duan, Q., Lei, X., Li, H., 2018. Spatiotemporal changes in extreme temperature and precipitation events in the Three-Rivers Headwater region, China. J. Geophys. Res. Atmos. 123 (11), 5827–5844.

Xia, J.Y., Niu, S.L., Ciais, P., et al., 2015. Joint control of terrestrial gross primary productivity by plant phenology and physiology. Proc. Natl. Acad. Sci. U. S. A. 112, 2788–2793.

Yang, B., He, M.H., Shishov, V., et al., 2017. New perspective on spring vegetation phenology and global climate change based on Tibetan Plateau tree-ring data. Proc. Natl. Acad. Sci. U. S. A. 114, 6966–6971.

Yu, H., Luedeling, E., Xu, J., 2010. Winter and spring warming result in delayed spring phenology on the Tibetan Plateau. Proc. Natl. Acad. Sci. 107, 22151–22156.

Zeng, J.Y., Li, Z., Chen, Q., Bi, H.Y., Qiu, J.X., Zou, P.F., 2015. Evaluation of remotely sensed and reanalysis soil moisture products over the Tibetan Plateau using in-situ observations. Remote Sens. Environ. 163, 91–110.

Zhang, Y.Q., Yu, Q., Jiang, J., Tang, Y.H., 2008. Calibration of Terra/MODIS gross primary production over an irrigated cropland on the North China Plain and an alpine meadow on the Tibetan Plateau. Glob. Chang. Biol. 14, 757–767.

Zhang, L., Zhao, F., Chen, Y., Dixon, R.N., 2011. Estimating effects of plantation expansion and climate variability on streamflow for catchments in Australia. Water Resour. Res. 47.

Zhang, G.L., Zhang, Y.J., Dong, J.W., Xiao, X.M., 2013. Green-up dates in the Tibetan Plateau have continuously advanced from 1982 to 2011. Proc. Natl. Acad. Sci. U. S. A. 110, 4309–4314.

Zhang, Y., Guanter, L., Berry, J.A., et al., 2014. Estimation of vegetation photosynthetic capacity from space-based measurements of chlorophyll fluorescence for terrestrial biosphere models. Glob. Chang. Biol. 20, 3727–3742.

Zhang, W.J., Yi, Y.H., Song, K.C., Kimball, J.S., Lu, Q.F., 2016a. Hydrological response of alpine wetlands to climate warming in the eastern Tibetan Plateau. Remote Sens. 8.

Zhang, Y., Xiao, X., Jin, C., et al., 2016b. Consistency between sun-induced chlorophyll fluorescence and gross primary production of vegetation in North America. Remote Sens. Environ. 183, 154–169.

Zhang, Q., Kong, D.D., Shi, P.J., Singh, V.P., Sun, P., 2018. Vegetation phenology on the Qinghai-Tibetan Plateau and its response to climate change (1982–2013). Agric. For. Meteorol. 248, 408–417.

Zhao, L., Li, Y.N., Xu, S.X., Zhou, H.K., Gu, S., Yu, G.R., Zhao, X.Q., 2006. Diurnal, seasonal and annual variation in net ecosystem CO2 exchange of an alpine shrubland on Qinghai-Tibetan plateau. Glob. Chang. Biol. 12, 1940–1953.

Zheng, Z.T., Zhu, W.Q., Chen, G.S., Jiang, N., Fan, D.Q., Zhang, D.H., 2016. Continuous but diverse advancement of spring-summer phenology in response to climate warming across the Qinghai-Tibetan Plateau. Agric. For. Meteorol. 223, 194–202.

Zhou, S., Zhang, Y., Caylor, K.K., et al., 2016. Explaining inter-annual variability of gross primary productivity from plant phenology and physiology. Agric. For. Meteorol. 226, 246–256.

Zhou, S., Zhang, Y., Ciais, P., et al., 2017. Dominant role of plant physiology in trend and variability of gross primary productivity in North America. Sci. Rep. 7, 41366.

Zhuang, Q., He, J., Lu, Y., Ji, L., Xiao, J., Luo, T., 2010. Carbon dynamics of terrestrial ecosystems on the Tibetan Plateau during the 20th century: an analysis with a process-based biogeochemical model. Glob. Ecol. Biogeogr. 19, 649–662.